THE JOURNAL OF PHYSICAL CHEMISTRY C
A JOURNAL OF THE AMERICAN CHEMICAL SOCIETY

pubs.acs.org/JPCC

Article

Introducing Novel Materials with Diffuse Electrons for Applications in Redox Catalysis and Quantum Computing via Theoretical Calculations

Published as part of The Journal of Physical Chemistry virtual special issue "Early-Career and Emerging Researchers in Physical Chemistry Volume 2".

Benjamin A. Jackson, Stephen G. Dale,* María Camarasa-Gómez, and Evangelos Miliordos*

Cite This: *J. Phys. Chem. C* 2023, 127, 9295−9308

Read Online

ACCESS | Metrics & More | Article Recommendations | Supporting Information

ABSTRACT: Diamond-like structures, where carbon atoms have been replaced with Li^+ and C−C bonds with diamines, have currently been introduced as new materials, which can host diffuse electrons in the periphery of each lithium tetra-amine center. These materials display a diverse range of properties behaving as metals or semiconductors depending on the diamine chain length. Multi-reference wavefunction and density functional theory calculations were employed to study the electronic structure of these materials. Initially, gas phase calculations are performed on isolated $(NH_3)_3LiNH_2(CH_2)_{1-10}H_2NLi(NH_3)_3$ molecular strings. One diffuse electron surrounds the periphery of each $-NH_2Li(NH_3)_3$ terminus. The two terminal electrons couple into a triplet and open-shell singlet states, which are nearly degenerate for long chains and as closed shell singlets for short. At intermediate lengths, the wavefunction of the ground-state singlet state mixes both open- and closed-shell configurations raising doubts about which configuration should be considered for density functional theory calculations. Observations from gas phase calculations accurately predict properties from the condense phase density functional theory calculations carried out for proposed crystalline Li-diamine materials, offering an avenue for further development and insight. Spin-polarized and unpolarized calculations are performed for the whole range of hydrocarbon sizes reporting geometrical and electronic band structures, spin density contours, and density of states. Diffuse electrons can be used for redox reactions or can serve as qubits for quantum computing. Future work will focus on decorating the hydrocarbon backbone with functional groups and/or bulky units, in order to facilitate or block the association between neighboring electrons for more controlled quantum computing applications and propose materials for selective redox catalysis.

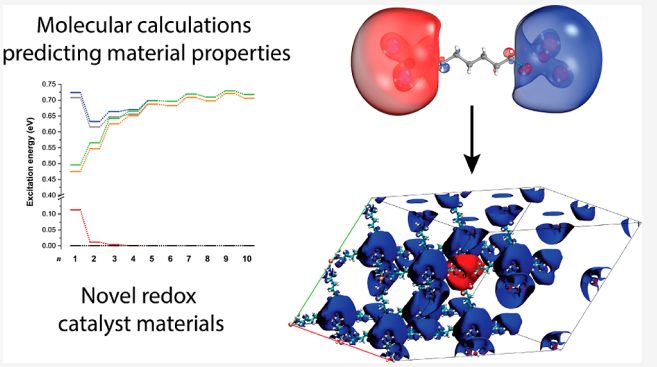

1. INTRODUCTION

Organic electrides and liquid (or expanded) metals are two families of materials that possess diffuse electrons localized in cavities or delocalized in a grid of positively charged metal complexes. The building units are typically complexes of alkali metals with crown-ethers (organic electrides) or ammonia (expanded metals).[1−5] The generation of the diffuse electrons can be seen as the migration of the metallic electrons to the periphery of the formed complexes displaced by the presence of the ligands.[6,7] For example, theoretical calculations show that only 6% of the density produced from the highest energy orbital occupied by the diffuse electron in $Li(NH_3)_4$ remains within the covalent radius of any of the atoms (Li: ∼2%, N: ∼1%, and H: ∼0.1%).[8] Further, experimental nuclear magnetic resonance measurements of Cs-crown-ether complexes find significantly depleted electron spin density of the metal center (0.063 and 0.03% for $Cs^+(15C5)_2.e^-$ and $Cs^+(18C6)_2.e^-$, respectively, compared to free Cs).[9] Within the alkali family, each metal center may have one electron displaced to produce a diffuse electron. Our recent computational findings on isolated (gas-phase) molecular ammonia complexes indicate that other metals (alkaline earth metals, transition metals, f-block elements, and even metalloids) can provide a larger number of diffuse electrons between one and three electrons observed to date.[7,10−14] These systems with ligand separated electrons, called solvated electron precursors (SEPs), are

Received: January 30, 2023
Revised: April 11, 2023
Published: May 9, 2023

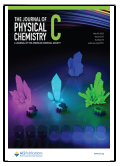

https://doi.org/10.1021/acs.jpcc.3c00675
J. Phys. Chem. C 2023, 127, 9295−9308

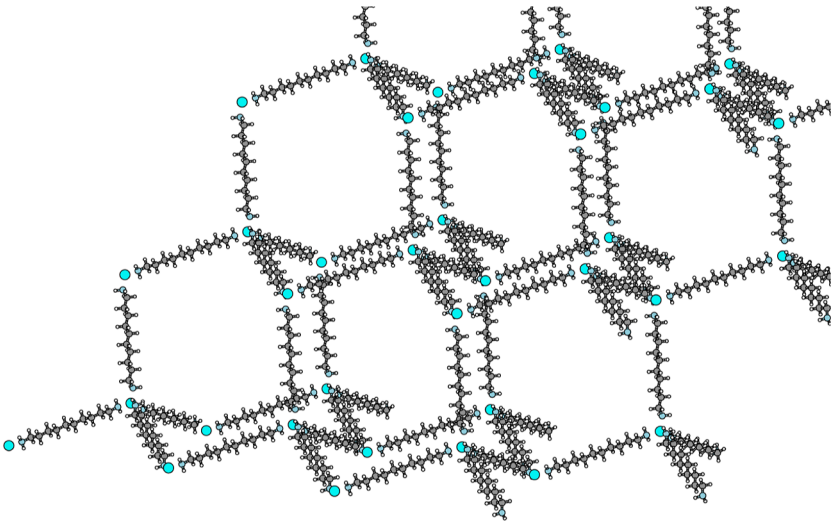

Figure 1. Three-dimensional crystal structure of the optimized *LiAmC10*.

observed in metal ammonia solutions of intermediate concentrations[15] and as stable gas phase complexes.[16,17] The properties of SEPs are determined by its two components: the identity of the metal center and of the ligands. Along the metal identity axis, thorium makes the most exotic species forming a $Th(NH_3)_{10}$ complex with four diffuse peripheral electrons (article in preparation). Moving along the second axis of the chemical space (ligand identity), water,[17−21] dimethyl ether,[22,23] crown ethers,[24−26] methanol,[27,28] cyclams,[29] cryptands,[29] methylated ammonia,[2,30−37] and diamines[24] have been shown to create similar systems with various coordination numbers, stabilities, and reactivity.

Our most recent work first identified the ability to chemically bind two SEP centers to create a linked dimer, which we refer to as linked-SEPs.[14,38] It identifies one method for linking SEPs by using aliphatic chains covalently bonded to each metal and sufficient ammonia ligands to displace the remaining metal valence electrons. Two systems were studied, $(NH_3)_3Be(CH_2)_{1-6}Be(NH_3)_3$ and $(NH_3)_3B(CH_2)_{3-6}B(NH_3)_3$, with each metal center offering one and two diffuse electrons for Be and B, respectively.[14,38] Our main observation was the bridged SEP centers act as two distinct atoms fixed at a distance determined by the carbon chain length. For example, the two electrons of $(NH_3)_3Be(CH_2)_{1-6}Be(NH_3)_3$ (one around each Be center) may couple to form either a triplet or singlet state. The two states are nearly degenerate and only for three carbon (and shorter) chains do the two electrons begin to couple into a closed-shell singlet, forming a bond analogous to σ-bonds in diatomic molecules. The wavefunction of these shorter chain lengths are multi-reference, including terms for both the open-shell and closed-shell singlet (see Section 3); in the shortest chain, the closed shell component increasingly dominates. In the case of $(NH_3)_3B(CH_2)_{1-6}B(NH_3)_3$, the two SEP centers resemble the interaction of two closed-shell He atoms.

Another method for bridging SEPs, we believe, is offered using diamine ligands. As evidenced, the SEP produced from the diamine bidentate complex $Li(H_2NCH_2CH_2NH_2)_2$ is shown to have a stability similar to the experimentally observed $Li(NH_3)_4$.[24] In addition, expanded metals composed of pure ammonia or methylamine lithium complexes, mixed $Li(NH_3)_x(NH_2CH_3)_{4-x}$ species, have been experimentally synthesized and structurally characterized, while their electronic structure has been examined theoretically.[2,30−37,39] As a natural extension of this work, we begin with the characterization of the molecular diamine-linked $(NH_3)_3LiNH_2(CH_2)_nH_2NLi(NH_3)_3$ dimers. The results of this leads us to propose a novel material produced by linking several Li-SEP centers with diamines. This crystalline material would be composed of a three-dimensional grid of Li centers bridged by $NH_2(CH_2)_nH_2N$ diamines (see Figure 1 for n = 10). For brevity's sake, the molecular linked-SEPs will, henceforth, be denoted as *LiAm-LSEP(n)*, while the crystalline structures will be denoted *LiAmCn* [e.g., *LiAm-LSEP(5)* and *LiAmC5*]. Here, *Li* denotes the metal center, *Am* is the amine linker, and *C* is the bridging chain to be of *n* carbons long. The n = 1−10 systems are studied.

As will be shown, the proposed crystalline material offers several intriguing characteristics and applications. One possible application for such materials is reduction−oxidation (redox) catalysis. The loosely bound electrons can reduce various molecular species, such as organic molecules (e.g., the Birch reduction with solvated electrons).[40,41] An important potential application is in carbon capture and sequestration methods through CO_2 conversion to industrial platform chemicals, such as methanol or lactones. We recently demonstrated that $Li(NH_3)_4$ can readily reduce CO_2 and stabilize the otherwise unstable CO_2^- anion due to interactions with the remaining $Li(NH_3)_4^+$ center.[42] The addition of H_2 or dienes converts the radical CO_2^- to methanol or lactones and the cycle closes by returning one electron to $Li(NH_3)_4^+$. This work investigated the use of $Li(NH_2CH_3)_4$ and $Li(NH_2CH_2CH_3)_4$, showing the carbon chain to have a negligible effect on the catalytic mechanism, providing evidence for potential applications of *LiAmCn* in a similar fashion. Further, the adjustment of the pore size (hydrocarbon chain length) and addition of functional or steric groups to the hydrocarbon backbone can render these materials highly selective.

A more ambitious use case pertains to quantum computing. Arrays of Rydberg atomic states have been proposed for quantum computing applications and have been shown to have several advantages due to the stronger atomic interactions, tunability, long life time, and stronger interactions (by 6 orders of magnitude) with electromagnetic fields.[43−45] The diffuse

https://doi.org/10.1021/acs.jpcc.3c00675
J. Phys. Chem. C 2023, 127, 9295−9308

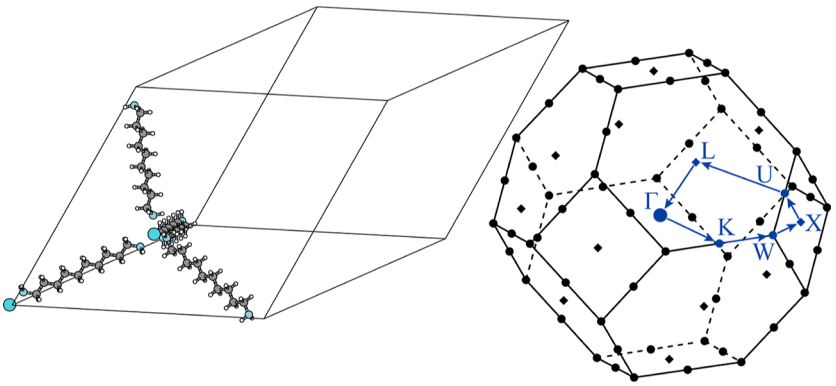

Figure 2. Left—the primitive cell of *LiAmC10* used for geometry optimizations and electronic band structure calculations. Right—the first Brillouin zone of the *LiAmC10* primitive cell and the k-path used for the band structure.

electron(s) of each metal center in the presently introduced systems are expected to have even better features as they are more polarizable and are present in the ground state. In addition, the decoration of the aliphatic scaffold with functional groups or bulky units can potentially facilitate or block the electron correlation between nearby SEP centers. We believe that the proposed materials are good candidates for scalable molecular spin-qubit systems[46,47] with similar synthetic flexibility compared to chromium organometallic crystals[48] while allowing for better control of quantum logic building blocks compared to strong mobile defects in those materials or in molecular wires[49,50] and are easier to scale compared to recent alternative propositions, such as spin-defects hosted in two-dimensional lattices.[51]

This work is a first exploration of a model system composed of Li^+ centers connected with diamines and surrounded by diffuse electrons (one for each Li^+ center). Our goal is to study first the electronic structure of the gas phase molecular species and then that of the condensed phase crystalline structure proposed here, providing a critical connection between the electronics of the two. To this end, we provide singlet−triplet splitting of *LiAm-LSEP(n)* dimers and electronic density maps, electronic band structure diagrams, density of states, projected density of states, and magnetic characterization of *LiAmCn*. A more detailed discussion of structural properties and temperature-dependent structural stability of *LiAmCn* will be addressed in a forthcoming paper (molecular dynamics studies).

2. COMPUTATIONAL DETAILS

2.1. Molecular Linked-SEPs. The geometry optimizations for *LiAm-LSEP(n)* $n = 1-10$ were performed with the density functional theory (DFT) and the CAM-B3LYP functional[52] combined with the aug-cc-pVDZ basis set[53−55] for all atoms [see Table S8 of Supporting Information for Cartesian coordinates]. CAM-B3LYP has been shown to provide geometries equivalent to MP2 and CCSD(T) geometries.[56] The triplet state (S = 1) was used for the optimization because it is single reference and is described by DFT better than the multi-reference singlet state (see Section 3—molecular linked SEPs). These geometries are used for all subsequent gas phase calculations. It should be mentioned that all carbon−carbon bonds have a staggered conformation. For similar Be species (see below and ref 38), we saw in the past that allowing other conformations (eclipsed or Gauche) for the singlet spin states may lead to (slightly) lower energy curved structures. Table S9 of Supporting Information shows that such structures are higher in energy within a few kcal/mol. It is unclear what conformation will be more stable for the crystalline species and may be temperature dependent. Presently, we consider only "linear" chains, but our ongoing molecular dynamics studies will provide more information.

The electronic structure analysis for the ground and low-lying excited states was done with multi-reference methods using MOLPRO.[57] The active space for the reference complete active space self-consistent field (CASSCF) calculations included the two diffuse electrons in eight orbitals representing the 1s, $1p_x$, $1p_y$, and $1p_z$ peripheral orbitals of each SEP unit. The dynamic correlation was obtained at the CASPT2 level promoting all valence electrons to the virtual space. To remove possible divergences caused by intruder states, a level shift value of 0.2 a.u. and an IPEA (shift parameter for orbital energies) value of 0.25 a.u. were applied.[58,59] The cc-pVDZ basis set was used for Li, N, and C, and the d-aug-cc-pVDZ for all H centers to describe the diffuse nature of the peripheral electrons.[53−55] Singly augmented basis sets were found adequate for the lowest energy electronic states but doubly augmented sets are suggested for higher energy states.[11] For the DFT calculations on the lowest singlet and triplet states with the Becke, 3-parameter, Lee−Yang (B3LYP),[60,61] and Perdew−Burke−Ernzerhof (PBE)[62] functionals, we used Gaussian16[63] and the cc-pVTZ (Li,N,C) aug-cc-pVTZ(H) sets.[53−55] Because we are only interested in low-lying states, singly augmented sets are considered proper for this study.

In addition, we preformed DFT calculations and applying periodic boundary conditions for *LiAm-LSEP(n)*, ($n = 1-5$), in which the species were centered within cubes sufficiently sized to ensure isolation from adjacent cells, ranging from 34 Å in length $n = 1$ to 41.5 Å $n = 5$; see Table S8 of Supporting Information for structures. These calculations were done using Quantum Espresso (QE)[64] with a uniformly spaced $2 \times 2 \times 2$ *k*-space grid, an 80 Ry cut-off energy, Gaussian smearing with a smearing temperature of 0.05 eV, spin polarization, and the PBE functional. Different spin states were obtained by setting initial magnetization of Li centers. In addition, the PBE, PBE0, and B3LYP functionals were tested using Fritz Haber Institute "Ab initio molecular simulations" (FHI-aims).[65] The methodology employed is discussed in more detail in the subsequent section.

2.2. Crystalline Linked-SEPs. Initial geometries for the crystalline structure of Figure 1 are constructed based on a "diamond" crystalline structure owing to the tetrahedral

https://doi.org/10.1021/acs.jpcc.3c00675
J. Phys. Chem. C 2023, 127, 9295−9308

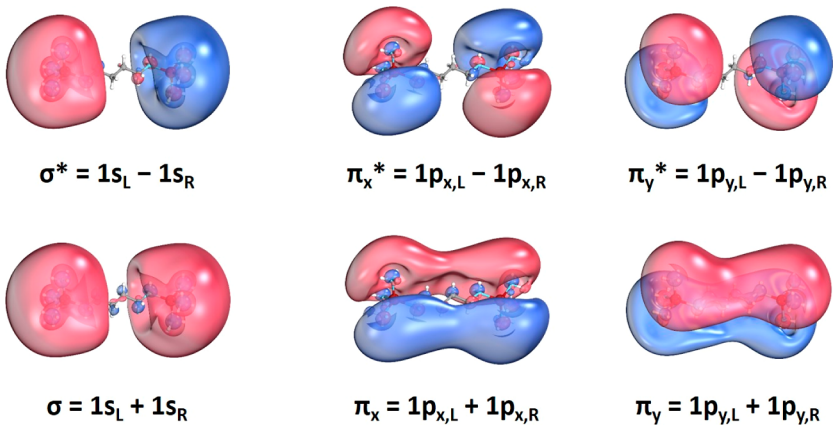

Figure 3. Lowest energy orbitals occupied by the diffuse electrons at the lowest energy electronic states of $(NH_3)_3LiNH_2(CH_2)_4H_2NLi(NH_3)_3$, and their composition in terms of the 1s, $1p_x$, and $1p_y$ orbitals of the two SEP centers (R = right, L = left).

structure of $Li(NH_3)_4$. The initial geometry of the linking diamine chains was obtained from the gas-phase calculations. Both the cell parameters and atomic positions were optimized with the subsequent DFT calculations using periodic boundary conditions in QE; see below for more details. The primitive unit cell was employed for the optimization, which contains two Li atoms and four linker diamine molecules (see Figure 2).

The periodic DFT calculations were carried out with the PBE functional with two different approaches: (1) the plane waves/pseudopotentials (PW/PS) approach and the projected augmented wave (PAW) formalism under periodic boundary conditions[66] as implemented in QE computational package[64] and (2) the numerically tabulated atom-centered basis sets as implemented in the FHI-aims computational package.[65] In addition, for FHI-aims the PBE0 and B3LYP functionals were also tested. For brevity's sake, we will refer to the different methodologies as program/functional, e.g., FHI-aims/PBE and QE/PBE. The various methods (QE/PBE, FHI-aims/PBE, FHI-aims/PBE0, and FHI-aims/B3LYP) were used to determine whether a consistent description could be obtained across methodological variation, especially because systems with diffuse electrons are known to be sensitive to such changes;[67−69] which computational package was used for which data will be highlighted throughout this work when pertinent. For QE calculations, an 86 Ry cut-off energy (ecutwfc = 86, ecutrho = 860), Gaussian smearing with a smearing temperature of 0.05 eV, and spin-polarization was used (see Table S11). The *k*-point mesh varied by chain length with higher mesh densities used for shorter chain lengths (see Table S10 of the Supporting Information for details). When using FHI-aims, the tight settings/tier2 basis set was used with a uniform 4 × 4 × 4 *k*-points mesh and a Gaussian smearing of 0.05 eV. The Pulay mixer with a charge mixing parameter of 0.01 was employed to aid convergence.[70]

Three distinct electronic systems were identified, the spin-unpolarized and spin-polarized which is ferromagnetic or antiferromagnetic. The choice of magnetic state was made by setting an initial magnetization of −1 on one Li atom and +1 on the other for the antiferromagnetic state or +1 on both for the ferromagnetic. Magnetization on the NH_2− hydrogens was also tested and produced identical ferromagnetic/antiferromagnetic solutions. For *LiAmC1*−*LiAmC3*, only the spin-unpolarized configurations were observed regardless of applied magnetization. For *LiAmC4* and *LiAmC5*, all three spin states were obtained and their optimized crystal structures were compared using a measure of similarity between powder spectra[71] as implemented in critic2.[72] In all examined cases, this test revealed negligible differences between each crystal structure. Therefore, only the unpolarized states of *LiAmC6*−*LiAmC10* were optimized, and these geometries were used for all subsequent calculations due to the high computational cost. The structure of all unit cells is provided in a GitHub repository listed in the Supporting Information. K-paths used in electronic band structure calculations were generated using XCrySDen[73] and are also in the GitHub repository. Figures include images generated from the VMD[74] and IboView[75] software.

The work here spans molecular and crystalline systems and similarly spans a wide energy range from large singlet−triplet gaps (up to 1 eV) to small magnetic energy differences (2×10^{-5} eV). To ease discussion and acknowledge the different fields originating from the methods used, relative energies will be discussed in eV for differences greater than 0.5 eV, in *K* for those less than 0.001 eV, and in cm^{-1} otherwise. Respecting convention, band gap energies E_G will always be referenced in eV.

3. RESULTS AND DISCUSSION

3.1. Molecular Linked-SEPs. We first focus on the electronic structure of two lithium SEPs connected with a diamine of various carbon chain lengths, *LiAm-LSEP(n)* with *n* = 1−10. We compare our results with similar species we studied recently $(NH_3)_3BeCH_2(CH_2)_nH_2CBe(NH_3)_3$, where the lithium atoms are replaced with beryllium and the NH_2 units with CH_2 to keep one outer diffuse electron around each metal center.[38] The frontier peripheral orbitals occupied by the diffuse electrons are of identical nature for the two species; the orbitals of *LiAm-LSEP(4)* are depicted in Figure 3. $(NH_3)_3BeCH_2(CH_2)_nH_2CBe(NH_3)_3$ can be seen as the linked analogue of two $(NH_3)_3BeCH_3$ moieties.[38] To this end, we refer to Be linked-SEP dimers as *BeMe-LSEP(n)*, where "*Me*" signifies the methyl groups bound to each Be and *n* denotes the carbon chain length linking these methyl groups. Therefore, $(NH_3)_3BeCH_2(CH_2)_3H_2CBe(NH_3)_3$ is two $(NH_3)_3BeCH_2$− moieties bridged by an aliphatic chain of three $-CH_2-$ to give *BeMe-LSEP(3)*.

For *BeMe-LSEP(n)* and *LiAm-LSEP(n)*, each SEP unit bears one diffuse electron in a pseudo-spherical s-type orbital, each center is analogous to a hydrogenic atom. As such, we can describe the interaction of these electrons within the

https://doi.org/10.1021/acs.jpcc.3c00675
J. Phys. Chem. C 2023, 127, 9295−9308

framework of bonding in H_2. The electrons of two hydrogen atoms may couple into a singlet (S = 0) or triplet (S = 1). The wavefunctions of these two spin-states at large H−H separations are as follows

$$|\Psi_{S=0;M_S=0}\rangle = \frac{1}{\sqrt{2}}(|1s_R\overline{1s_L}\rangle - |\overline{1s_R}1s_L\rangle) \quad (1)$$

$$|\Psi_{S=1;M_S=1}\rangle = |1s_R 1s_L\rangle \quad (2)$$

where R and L denote the right and left H atoms or SEP units and kets denote Slater determinants. The $1s_R$ and $\overline{1s_R}$ notation denotes α and β spins, respectively. Due to the inherent symmetry in the Hamiltonian (the two units are symmetry equivalent), the $1s_R$ and $1s_L$ localized orbitals are mixed into the "bonding" and "anti-bonding" orbitals $\sigma = N_+(1s_R + 1s_L)$ and $\sigma^* = N_-(1s_R - 1s_L)$, respectively ($N_+ = N_- = 1/\sqrt{2}$ at long separations). In the σ/σ^* basis, the same two wavefunctions are written equivalently as[76]

$$|\Psi_{S=0;M_S=0}\rangle = \frac{1}{\sqrt{2}}(|\sigma\,\overline{\sigma}\rangle - |\sigma^*\,\overline{\sigma^*}\rangle) \quad (3)$$

$$|\Psi_{S=1;M_S=1}\rangle = |\sigma\,\sigma^*\rangle \quad (4)$$

In the case of H_2, the triplet state is repulsive, whereas the singlet state produces the strongly bound ground state. The wavefunction of the triplet state retains its form as the two H atoms approach. Conversely, the weight for the first term of the singlet state ($\sigma\,\overline{\sigma}$ or σ^2) increases gradually and dominates at the equilibrium distance forming the H−H covalent bond. The singlet−triplet splitting in H_2 sharply increases as we move to shorter distances.[77,78]

In contrast to H_2, the two SEP units in *LSEPs* can be fixed at specific distances determined by the number of carbon atoms of the linker diamine molecule. Our calculations reveal the exact same trends as in H_2. The wavefunctions are given by eqs 3 and 4 for long hydrocarbon chains, the triplet wavefunctions remains the same as in eq 2, but the singlet is better described as

$$|\Psi_{S=0;M_S=0}\rangle = N\,(c_1|\sigma\,\overline{\sigma}\rangle - c_2|\sigma^*\,\overline{\sigma^*}\rangle) \quad (5)$$

where N is a normalization constant and c_1 and c_2 vary with the linker's length. When coefficients c_1 and c_2 are equal, we have a pure diradical species. For cases of $c_1 \geq c_2$, diradical character β_r is determined as[76,79,80]

$$\beta_r = \frac{2c_2^2}{c_1^2 + c_2^2} \quad (6)$$

The value of β_r is 1 when $c_1 = c_2$ and 0 when $c_2 = 0$. Table 1 lists our c_1, c_2, β_r, and singlet−triplet splitting ΔE for lithium diamine linked-SEPs (*LiAm-LSEPs*) with up to 10 carbon atoms. Figure 3 shows the contours for σ and σ^* orbitals for n = 4, and Figure 4 plots β_r and ΔE with respect to the number of carbon atoms in the linker diamine. Figure 4 clearly shows a decrease in a diradical character from *LiAm-LSEP(10)* to *LiAm-LSEP(1)*, ranging from (β_r = 0.999 or 99.9%) to (β_r = 0.198 or 19.8%). Singlet−triplet splitting inversely correlates with chain length, with the largest for n = 1 at 783.9 cm^{-1} dropping to <1 cm^{-1} for $n \geq 6$. For a comparison, the singlet−triplet splitting for the H_2 molecule is 85562 cm^{-1} at equilibrium.[77]

Table 1. CASPT2/cc-pVDZ(Li, N, C), d-aug-cc-pVDZ(H) Singlet−Triplet Splitting (ΔE, cm^{-1}), Normalization Constants (c_1, c_2), and Diradical Character (β_r) for *LiAm-LSEP* and *BeMe-LSEP* Species as a Function of n the Number of Linker Atoms in Chains

	LiAm-LSEP(n)				*BeMe-LSEP(n)*[a]	
n	c_1	c_2	β_r	ΔE[b]	β_r	ΔE
−1					0.165	3052.4
0					0.852	164.5
1	0.8800	0.2915	0.198	783.9	0.855	86.7
2	0.8327	0.4897	0.514	126.9	0.994	−0.2
3	0.7774	0.6089	0.760	45.2	0.988	0.6
4	0.7395	0.6657	0.895	8.5	1.000	0.03
5	0.7237	0.6863	0.947	2.8		
6	0.7142	0.6979	0.977	0.4		
7	0.7106	0.7024	0.988	0.1		
8	0.7084	0.7051	0.995	−0.01		
9	0.7077	0.7061	0.998	−0.01		
10	0.7072	0.7067	0.999	−0.01		

[a]Reference 38. [b]Positive value indicates that the singlet state is lower in energy.

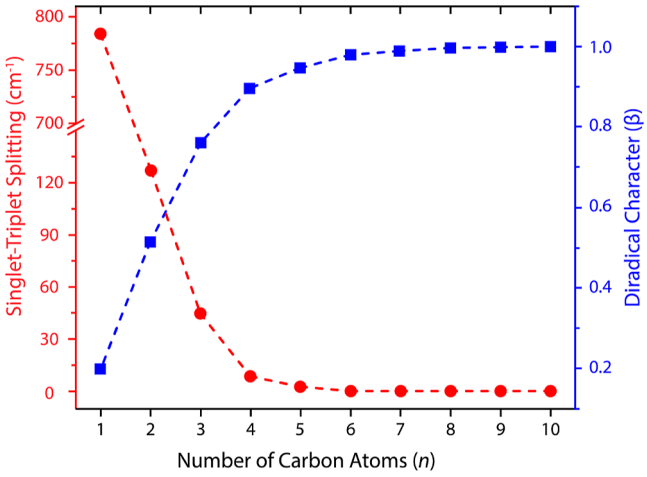

Figure 4. CASPT2/cc-pVDZ(Li,N,C), d-aug-cc-pVDZ(H) singlet−triplet splitting (left axis and red circles and line), and diradical character β_r (left axis and blue squares and lines) for the $(NH_3)_3LiNH_2(CH_2)_nH_2NLi(NH_3)_3$ species (n = 1−10).

The replacement of the SEP unit from $(NH_3)_3LiNH_2-$ to $(NH_3)_3BeCH_2-$ changes the electronic structure dramatically. For n = 1, the diradical character for the latter is already 85.5% with a splitting of 86.7 cm^{-1} (see Table 1 and ref 38). For $n \geq 2$, the two electrons are effectively coupled into an open-shell singlet ($\beta_r \sim 1$, $\Delta E \sim 0$). The reason for this is that the diffuse electron of each $(NH_3)_3BeCH_2-$ complex is polarized away from the chain to avoid the $-CH_2-$ side. This minimizes the overlap of the $1s_R$ and $1s_L$ orbitals. On the other hand, the $(NH_3)_3LiNH_2-$ complex distributes the density of the diffuse electron nearly evenly which facilitates the mixing of the $1s_R$ and $1s_L$ orbitals. This favors the σ^2 configuration, decreasing the diradical character, and increasing the singlet−triplet splitting. If we remove one CH_2 unit from *BeMe-LSEP(1)* and make $(NH_3)_3BeCH_2-CH_2Be(NH_3)_3$ (n = 0 in Table 1), the diradical character remains practically the same (85.2%) but ΔE doubles (164.5 cm^{-1}; see Table 1). Removing an additional CH_2 to give $(NH_3)_3Be-CH_2-Be(NH_3)$ (n = −1

https://doi.org/10.1021/acs.jpcc.3c00675
J. Phys. Chem. C 2023, 127, 9295−9308

in Table 1), β_r is nearly equal to that of *LiAm-LSEP(1)* at 16.5% and ΔE soars to 3052.4 cm^{-1}. Conclusively, N−H bonds along the linking molecule promote electronic conduction, whereas C−H bonds isolate the two diffuse electrons, increase bi-radical character, and decrease ΔE. Based on these results, we can conclude that molecular linked-SEPs bridged through covalent methyl bonds significantly decrease the degree of correlation between SEP electrons compared to diamine bridges. We can expect that the same will hold true when moving to crystalline linked-SEP materials.

Additionally, we examined the next four excited states of *LiAm-LSEPs*. Consistent with our previous works on *BeMe-LSEPs* and *BMe-LSEPs*,[14,38] these electronic states involve a promotion of one electron to the π and π^* orbitals of Figure 3. These are the constructive (+) and destructive (−) combinations of the $1p_x$ and $1p_y$ orbitals of the SEP termini. Computed excitation energies are plotted in Figure S12 of the Supporting Information and illustrate the $(\sigma, \sigma^*)^2$ states to be well separated from those including the occupation of π and π^* orbitals. For $n = 1$, excitation to the state $\sigma^1\pi^1$ occurs at ∼0.48 eV (3871.5 cm^{-1}) and increases to ∼0.71 eV (5726.5 cm^{-1}) for $n = 10$. Summarizing, CASSCF/CASPT2 results for *LiAm-LSEPs* show ground-state $(\sigma, \sigma^*)^2$ orbitals are produced from mixtures of SEP 1s orbitals and negligible hybridization of higher orbitals, e.g., 1p. In this work, we initially focus on molecular *LiAm-LSEPs* as an entry point for understanding the structure of condensed phase linked-SEPs. Experimental benchmarking and higher level computational methods, such as CASPT2, have shown that ground-state gas-phase SEPs may be well described with the DFT.[56] The question then is whether this accuracy extends to the proposed crystalline linked-SEPs, and whether the commonly employed PBE functional suitably describes these systems. Further, will gas phase results for molecular linked-SEPs allow the prediction of electronic properties of the corresponding crystalline form?

To address these questions, first we perform DFT calculations on a single *LiAm-LSEP(n)* molecule for two functionals: B3LYP, a functional often used for gas-phase calculations, and PBE, which is standard in condensed-phase calculations. We also perform DFT calculations with the PBE functional and applying periodic boundary conditions for the system of well-separated *LiAm-LSEP(n)* molecules (see Section 2). The primary issue with the use of DFT lies in describing the electronic structure of the singlet spin state, which we demonstrate in the previous section to be multireference in character, a mixture of closed-shell and open-shell (diradical) states. DFT methods assume a single Slater determinant is sufficient representation of an electronic state, which is insufficient to reproduce multireference character like that seen above for *LiAm-LSEPs*. Therefore, we considered both restricted-DFT (S = 0R) and unrestricted-DFT (S = 0U) calculations, or, equivalently, the unpolarized (S = 0R) and polarized-antiferromagnetic (S = 0U) periodic calculations, respectively.

Table 2 lists energy differences between the two "types" of singlets and the triplet states. For $n = 1$, the CASPT2 wavefunction was found primarily to be closed shell (β_r = 19.8%), and this reflects to the DFT/PBE calculations. For both gas and condensed phase PBE calculations, the S = 0U calculation converges to the S = 0R solution, i.e., the α and β orbitals are identical to σ. On the other hand, B3LYP predicts the S = 0R higher than the S = 0U by 77.9 cm^{-1}.

Table 2. Relative Energies of the Restricted Singlet (S = 0R) and Triplet States (cm^{-1}) with Respect to the Unrestricted Singlet (S = 0U) of *LiAm-LSEP(n)* for ($n = 1-5$) with Various Methods

	CASPT2	DFT/B3LYP		DFT/PBE		QE/PBE[c]	
N	S = 1	S = 1	S = 0R	S = 1	S = 0R	S = 1[a]	S = 0R[b]
1	783.9	973.1	77.9	1451.9	0.0		0.0
2	126.9	117.1	1043.6	116.6	318.0	49.4	313.0
3	45.2	42.6	1435.2	28.1	524.7	−21.5	425.3
4	8.5	10.2	1772.2	0.2	720.7	−24.8	530.7
5	2.8	3.6	1939.8	0.1	780.4	−15.1	561.8
	CASPT2	FHI-aims/PBE[c]		FHI-aims/PBE0[c]		FHI-aims/B3LYP[c]	
n	S = 1	S = 1[a]	S = 0R[b]	S = 1[a]	S = 0R[b]	S = 1[a]	S = 0R[b]
1	783.9		0.0		0.0		0.0
2	126.9	24.6	333.7	9.0	1660.5	28.4	1261.1
3	45.2	6.9	391.5	3.1	1192.6	13.3	835.1
4	8.5	0.0	428.0	−1.0	1553.5	3.2	1134.1
5	2.8	0.5	432.1	−0.4	1547.3	0.6	1115.3

[a]Polarized ferromagnetic with respect to the polarized antiferromagnetic (S = 0U). [b]Unpolarized with respect to the polarized antiferromagnetic (S = 0U). [c]Under periodic boundary conditions.

For $n > 1$, the S = 0U is always lower in energy than S = 0R. PBE predicts a smaller energy difference between S = 0U and S = 0R. This energy difference increases for larger n which agrees with the fact that the S = 0R part diminishes for larger n in the CASPT2 wavefunction. The S = 0U is also lower than the S = 1 state and becomes degenerate (within 10 cm^{-1}) for $n \geq 5$ for both B3LYP and PBE, which agrees with the CASPT2 results. Interestingly, with periodic boundary conditions QE/PBE erroneously predicts a ferromagnetic (S = 1) ground state configuration, the same is not true for FHI-aims/PBE, FHI-aims/PBE0, and FHI-aims/B3LYP which correctly predict the spin-polarized antiferromagnetic (S = 0U) ground state configuration. In all cases, the DFT results under periodic boundary conditions reproduces the trend of approaching degeneracy for increasing chain length and comparable ΔE for the singlet−triplet splitting relative to CASPT2. Overall, this suggests DFT to be a safe choice for *LiAm-LSEP(n)* when $n = 1$ and $n \geq 4$, where the wavefunction is clearly of S = 0R ($n = 1$) or S = 0U ($n \geq 4$). Extending this to *LiAmCn*, we can predict a similar conclusion to hold where carbon chains that are very short with highly coupled SEPs and long chains with well-separated SEP centers will be adequately described using DFT and the PBE functional but intermediate chain lengths less so. Further, we can anticipate QE/PBE to over stabilize the spin-aligned ferromagnetic state (S = 1).

Before switching our discussion to the condensed phase results, an important observation is in order pertaining to the composition and energy of the *LiAm-LSEP(n)* frontier orbitals for the S = 0U and S = 1 states obtained with DFT. The correct wavefunctions are given in eqs 1 and 2 [$1s_R/1s_L$ basis] or eqs 3 and 4 [σ/σ^* basis], respectively. The wavefunction of S = 1 can be equivalently described as $|1s_R 1s_L\rangle$ or $|\sigma\ \sigma^*\rangle$. The σ, σ^* orbitals are orthogonal, and their energy difference is zero at infinite separations and increasingly large at short distances. Due to the imposed orthogonality within the α-orbitals, our calculations converge to the $|\sigma\ \sigma^*\rangle$ Slater determinant. As far as the open-shell singlet state is concerned, the α and β electrons allows the "symmetry-broken" $|1s_R\ \overline{1s_L}\rangle$ solution, and the S = 0U state converges to a $|1s_R\ \overline{1s_L}\rangle$ Slater

https://doi.org/10.1021/acs.jpcc.3c00675
J. Phys. Chem. C 2023, 127, 9295−9308

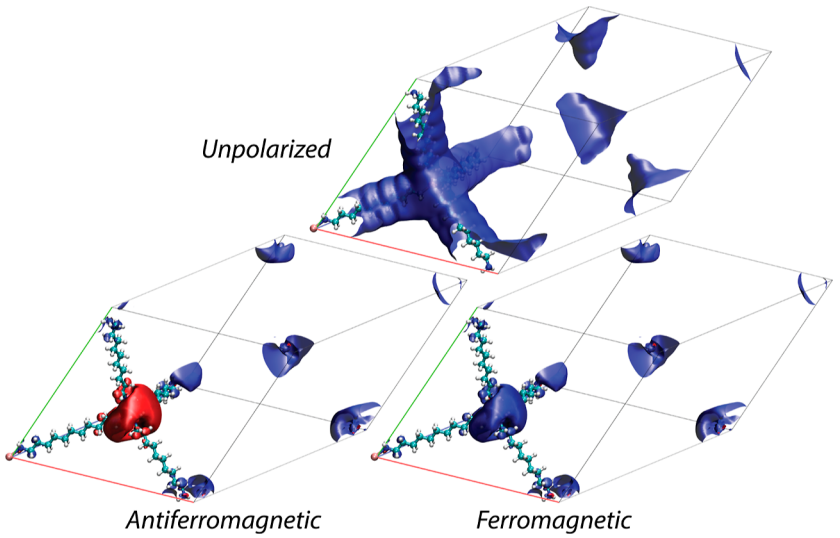

Figure 5. Electronic density of the spin unpolarized and polarized antiferromagnetic or ferromagnetic states of *LiAmC10* as calculated using FHI-aims and the PBE functional. Plotted with an isovalue of ±0.0002 a.u. For the spin polarized, red denotes the β and blue the α density.

Table 3. Relative Energies (cm^{-1}) for the Singlet (S = 0R and S = 0U) and Triplet (S = 1) States (cm^{-1}) of *LiAmCn* (*n* = 1−10) with Various Methods, Denoted as Program/Functional[a]

	QE/PBE			FHI-aims/PBE			FHI-aims/PBE0			FHI-aims/B3LYP	
n	S = 0U[b]	S = 1[c]	S = 0R[d]	S = 0U[b]	S = 1[c]	S = 0R[d]	S = 0U[b]	S = 1[c]	S = 0R[d]	S = 0U[b]	S = 1[c]
1			0.0			0.0			0.0		
2			0.0			0.0			0.0		
3	0.0	N/A[e]	27.8	0.0	275.2	188.8	0.0	201.7	1537.4	0.0	258.5
4	0.0	33.3	507.4	0.0	16.9	1017.4	0.0	25.4	N/A[e]	0.0	47.1
5	0.0	91.4	181.6	0.0	41.1	663.2	0.0	8.6	2731.2	0.0	32.4
6	0.0	−42.0	436.9	0.0	3.5	876.8	0.0	1.0	3119.5	0.0	3.8
7	0.0	−38.5	331.3	0.0	2.7	754.8	0.0	−4.1	3186.5	0.0	1.3
8	0.0	−16.6	179.4	0.0	0.0	481.9	0.0	−0.4	3084.6	0.0	0.6
9	0.0	−7.7	403.3	0.0	0.0	759.5	0.0	0.1	3446.8	0.0	0.1
10	0.0	−1.3	537.5	0.0	0.0	885.7	0.0	4.4	3735.7	0.0	−0.8

[a]For *n* = 1−2, QE and FHI-aims only produces an unpolarized, closed-shell (S = 0R) state. [b]Spin-polarized antiferromagnetic. [c]Spin-polarized ferromagnetic. [d]Unpolarized. [e]Unavailable due to convergence issues.

determinant failing to provide the correct spin-adapted form of eq 1. It appears that the $1s_R$ and $1s_L$ orbitals are consequently equivalent and have the exact same energies. The orbital energies for S = 1 and S = 0U for DFT/PBE are listed in Table S7 of the Supporting Information. These observations will reflect to the electronic band structure of the crystalline *LiAmC1*−*LiAmC10* species (see Section 3—crystalline linked-SEPs).

The smaller singlet−triplet gaps in the DFT can be attributed to the different delocalization error in the two states induced by the different occupied orbitals (σ/σ^* vs $1s_R/1s_L$).[81] The delocalization error (absent for CASPT2) can cause inaccurate energy and density descriptions of a system. Dale and co-workers have previously conducted work to ensure that valid qualitative studies on diffuse and localized electron systems can still be conducted reliably (see refs 67 and 82 and citations contained therein). Hybrid functionals (such as B3LYP or PBE0) can mitigate some of the effects of delocalization error,[82] but they are computationally more demanding than PBE (a GGA functional). Consistency between the PBE and PBE0 functionals would be a strong indicator of reliable calculations. To address this for *LiAmCn*, we provide not only DFT/PBE results from two different solid-state computational chemistry packages with different methodologies for orbital descriptions but also for FHI-aims we provide PBE, PBE0, and B3LYP results. Recent advances in both computational power, the efficiency of the FHI-aims code make these solid-state hybrid functional calculations practical, where they were not previously.

3.2. Crystalline Linked-SEPs. The various systems of *LiAmCn* may be divided into three categories: the long chains (*n* = 10−6), the intermediate chains (*n* = 5−3), and the short chains (*n* = 1−2). We begin with the discussion of the long chains. In Figure 2, the optimized cell and geometry of *LiAmC10* is shown. Three distinct electronic states are obtainable for this system: the spin-polarized ferromagnetic or antiferromagnetic states and the spin-unpolarized non-magnetic state; the electronic density of each is shown in Figure 5. The spin-polarized states depict a unit cell containing two isolated SEPs with an electronic structure analogous to a lone $Li(NH_3)_4$ or $(NH_3)_3Li(NH_2)-$ each possesses one solvated electron occupying a diffuse s-type orbital, surrounding the periphery of the $Li(NH_2-)_4$ center; the effect of the diamine ligands cause the diffuse SEP electrons to be polarized away from the chains into the direction of the voids within the

https://doi.org/10.1021/acs.jpcc.3c00675
J. Phys. Chem. C 2023, 127, 9295−9308

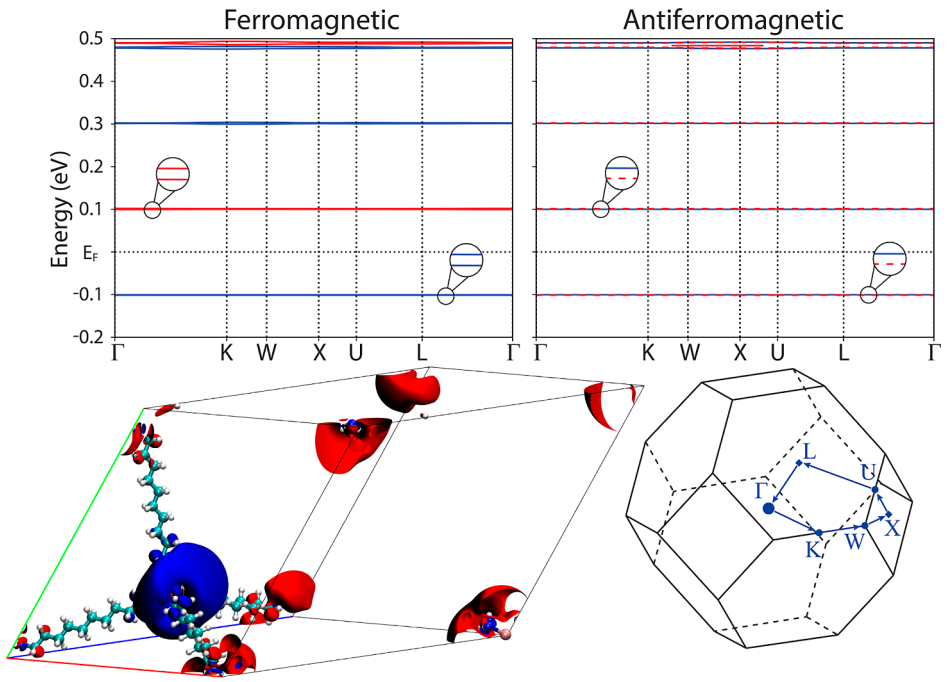

Figure 6. Shown is the band structure of *LiAmC10* computed using FHI-aims/PBE. Red denotes the β and blue the α spin channels. The structure of the Brillouin zone and the k-path used for band calculations is given. The bottom left figure depicts the local density of states for antiferromagnetic *LiAmC10* in the energy range of $(-0.2-E_F)$ calculated at QE/PBE. Note that figure insets for the band structure are added to emphasize that two degenerate bands coincide at −0.1 and 0.1 eV.

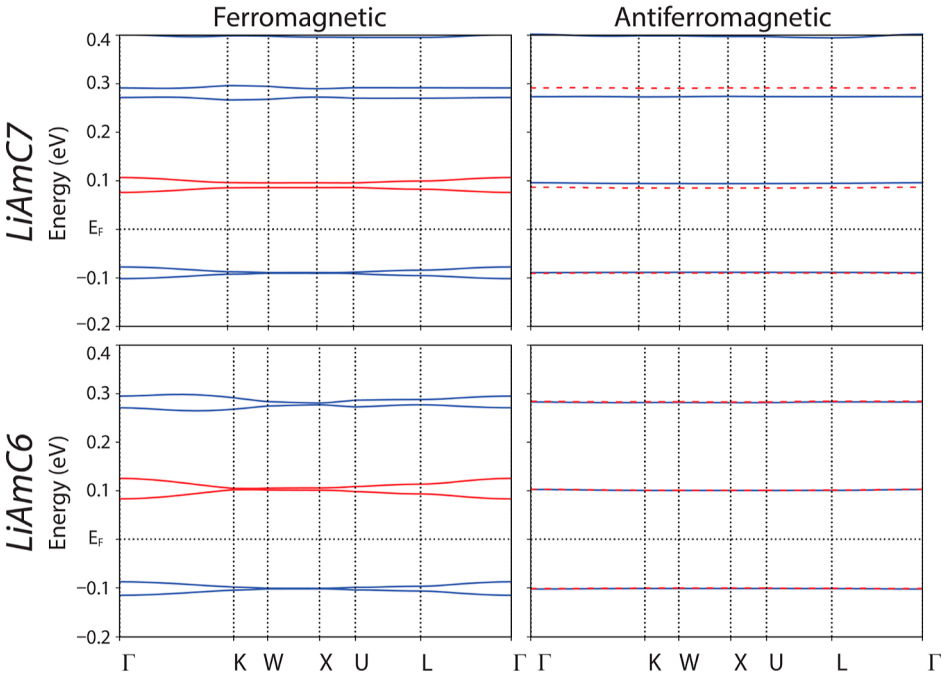

Figure 7. Shown is the band structure of *LiAmC7* and *LiAmC6* computed using FHI-aims/PBE. Red denotes the β and blue the α spin channels. For the Brillouin zone refer to Figure 6.

lattice. However, the diffuse electron remains localized to the space immediately around the lithium-amine center.

The two separate electrons may couple with the same spin to give the ferromagnetic or opposite spins to give the antiferromagnetic: analogous to the triplet (S = 1) and open-shell singlet (S = 0U) in *LiAm-LSEP(n)*, respectively. At this separation, the association between the two electrons is minimal and the two states are nearly degenerate (see Table 3). The spin-unpolarized solution requires adjacent centers to couple in σ-type bonding. However, the large separation of the adjacent centers significantly destabilizes this state, it is less stable by 885.7 and 3735.7 cm^{-1} as calculated using FHI-aims with the PBE and PBE0 functionals (Table 3). This holds true for all chain length $n \geq 3$, the unpolarized state is significantly higher in energy relative to the spin-polarized states.

https://doi.org/10.1021/acs.jpcc.3c00675
J. Phys. Chem. C 2023, 127, 9295−9308

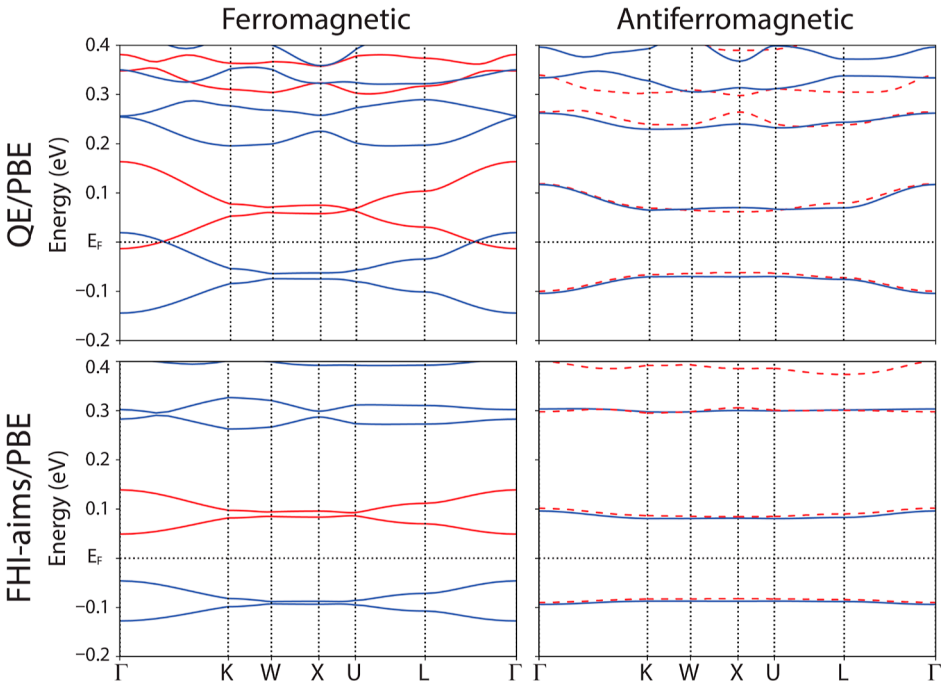

Figure 8. Band structure of *LiAmC5* computed using FHI-aims/PBE and QE/PBE. Red denotes the β and blue the α spin channels. For the Brillouin zone refer to Figure 6.

The calculated band structure for n = 10 of Figure 6 shows the bands of the ferromagnetic and antiferromagnetic spin-polarized states. The valence band of these systems corresponds to the orbital occupied by the diffuse electron centered about the lithium−amines, depicted by the local spin density in Figure 6. Examining the band structure of both states, it is clear that the α and β bands of each are identical. Further, these bands are nearly flat, and the two states are effectively degenerate (Table 3). Further, the morphology of the band structure and plotted electron density illustrate the valence band is produced from isolated SEP 1s orbitals which see no meaningful hybridization with higher energy 1p orbitals. This agrees with the orbital structure seen for *LiAm-LSEPs* in the previous section. Altogether, we can view the two electrons at this distance (r_{Li-Li} = 15.997 Å) occupying orbitals equivalent to isolated SEPs which negligibly interact with the other.

As the carbon chain becomes shorter, we see the degeneracy of the two α valence bands shown in Figure 6 is lifted only in the ferromagnetic case (see Figure 7). The same is observed for the corresponding triplet spin *LiAm-LSEP(n)* gas-phase species and results from the orthogonality of the occupied orbitals (σ, σ^*), see above and Table S7 of Supporting Information. In the anti-ferromagnetic or the corresponding singlet spin *LiAm-LSEP(n)* species, the two occupied orbitals are not orthogonal and are localized separately on the two SEP centers (unrestricted or polarized calculations). Their identical nature leads to the observed degeneracy of the α and β valence bands across the k-space.

Throughout the n = 6−10 range, the spin-polarized states are effectively degenerate with the singlet−triplet splitting as ∼0 cm^{-1} (n = 8−10), 2.7 cm^{-1} (n = 7), and 3.5 cm^{-1} (n = 6) at FHI-aims/PBE (Table 3). Application of hybrid functionals PBE0 and B3LYP all effectively give the same result with relative energies ranging between 0 and 4 cm^{-1} for n = 10−6 (see Table 3).

Comparing the electronic band structures produced from the various methods tested, we see that FHI-aims/PBE, FHI-aims/PBE0, and FHI-aims/B3LYP, all show a remarkable agreement in the morphology of the antiferromagnetic and ferromagnetic band structures (see Figures S1−S8 of the Supporting Information). Moving from PBE to the hybrid functionals PBE0 and B3LYP, the band gap E_G for all n = 6−10 increases significantly. For example, the E_G of *LiAmC10* increases from 0.20 to 1.03 and 0.82 eV for FHI-aims/PBE, FHI-aims/PBE0, and FHI-aims/B3LYP, respectively (see Table S6 of the Supporting Information). This behavior is to be expected; it is well understood that the "band gap problem" causes the PBE functional to significantly underestimate E_G and use of hybrid functionals tends to decrease this.[82] Comparing the band structure calculated with FHI-aims/PBE and QE/PBE, QE predicts a stronger interaction between SEP centers, as illustrated by the relatively "flat" bands of FHI-aims and the "curvy" bands of QE; this difference is minimal for n = 10−8 and increases markedly for n < 7 (see Figures S1−S4 of the Supporting Information).

An interesting note is QE, despite the strong agreement in E_g and band structure morphology, identifies the ferromagnetic S = 1 as the ground state for n > 5. Where FHI-aims predicts the ferromagnetic and antiferromagnetic as degenerate (within 4 cm^{-1}) for n > 5 for all functionals, QE/PBE predicts the ferromagnetic as lower by 42 cm^{-1} for n = 6. The ΔE decreases to 38.5, 16.6, 7.7, and 1.3 cm^{-1} for n = 7−10, respectively (see Table 3). This reflects the results of the gas-phase *LiAm-LSEPs* where QE/PBE also over-stabilized the ferromagnetic state.

Moving to our intermediate length chains (n = 3−5), the two spin-polarized states are no longer degenerate with the antiferromagnetic lower in energy by 41.1 and 16.9 cm^{-1} for n = 5 and n = 4, respectively (FHI-aims/PBE, see Table 3). It is for this group that we see the greatest discrepancy between the results of QE/PBE and FHI-aims/PBE. Comparing the band structure of the two methods for *LiAmC5*, we see this pattern

https://doi.org/10.1021/acs.jpcc.3c00675
J. Phys. Chem. C 2023, 127, 9295−9308

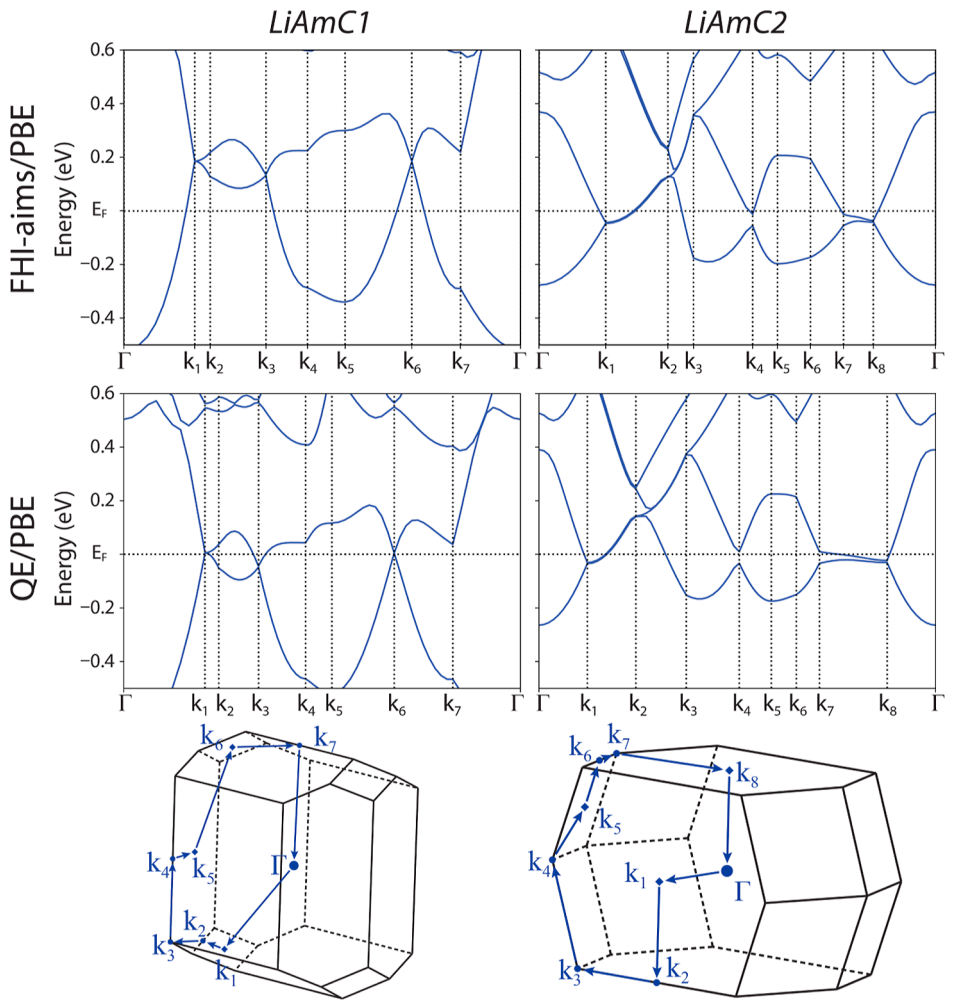

Figure 9. Band structure of *LiAmC2* and *LiAmC1* computed using FHI-aims/PBE and QE/PBE.

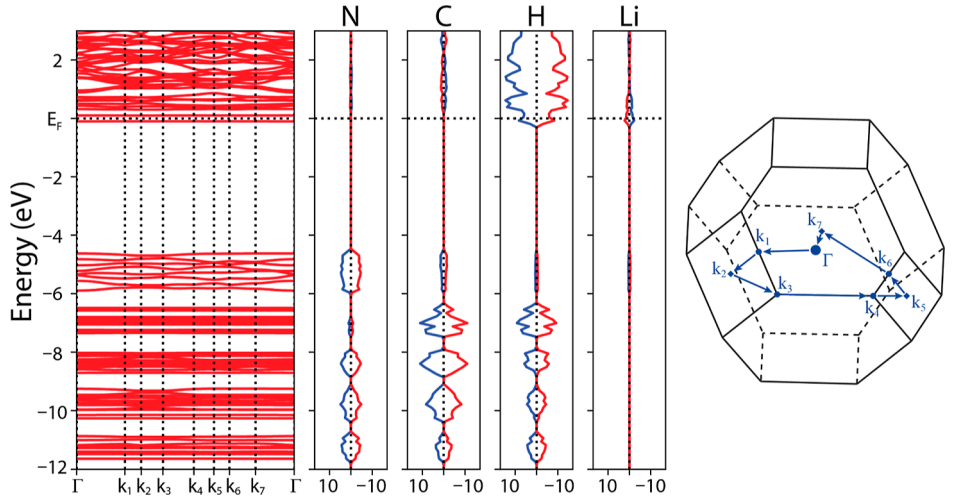

Figure 10. Plotted far-left is the electronic band structure of ferromagnetic *LiAmC4*. The middle plots correspond to the atomic-projected density of states for N, C, H, and Li. The α and β spin components are plotted in blue and red, respectively. The structure of the Brillouin zone and the k-path is given. The *x*-axis of the projected density of states is in units of $(\text{eV } V_{\text{unit cell}})^{-1}$.

of increasing divergence of α and β bands along K → Γ and L → Γ. However, the divergence markedly increases for the ferromagnetic QE/PBE leading to a crossing of the valence α and conduction β bands below the Fermi energy and a prediction of material with no band gap while FHI-aims/PBE predicts an E_G of 0.10 eV (see Figure 8). However, QE/PBE still predicts a band gap (E_G = 0.12 eV) for the antiferromagnetic. The FHI-aims/PBE band structure remains effectively flat for the valence and conduction bands, describing only weak interactions between adjacent cells. The different

https://doi.org/10.1021/acs.jpcc.3c00675
J. Phys. Chem. C 2023, 127, 9295−9308

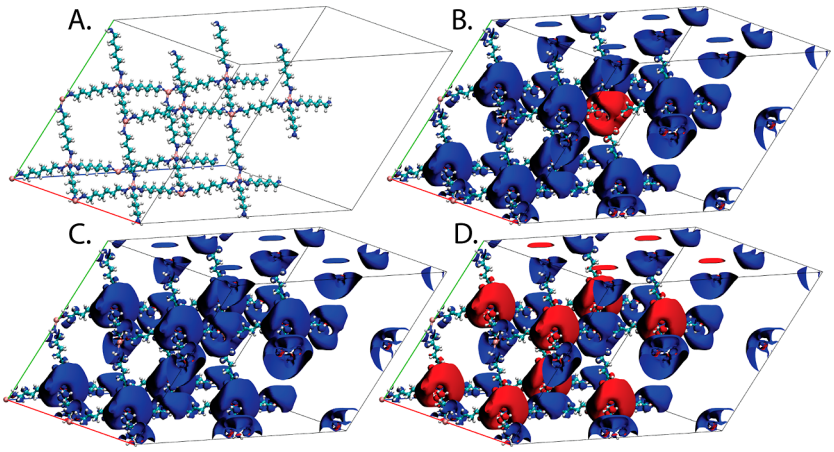

Figure 11. (A) Structure of *LiAmC6* 2 × 2 × 2 supercell containing 8 *LiAmC6* primitive cells and the spin density of (B) ferromagnetic with one spin flipped center, (C) ferromagnetic, and (D) antiferromagnetic. Red denotes the β and blue the α spin density.

functionals of FHI-aims agree in morphology- only increasing the band gap from 0.16 eV with PBE to 1.03 and 0.81 eV for PBE0 and B3LYP, respectively. The same observations hold true for *LiAmC4* and FHI-aims (see Figure S7).

For *LiAmC3*, we see a stronger agreement between FHI-aims and QE. The morphology of the band structure for QE/PBE and FHI-aims/PBE are near identical for both unpolarized and antiferromagnetic states (see Figure S8). E_G agrees at 0.07 and 0.13 eV for the antiferromagnetic at QE/PBE and FHI-aims/PBE, respectively. However, QE/PBE predicts a small absolute magnetization of 0.72 μB compared to 1.34 μB for FHI-aims (see Table S1). While QE/PBE can readily converge an antiferromagnetic state, we were unable to locate a true ferromagnetic state with all attempts converging to an unpolarized solution. QE/PBE favors this antiferromagnetic state by 27.8 cm^{-1} relative to the unpolarized result. Similarly, FHI-aims favors an antiferromagnetic (S = 0U) ground state with the unpolarized (S = 0R) higher by 188.8 cm^{-1} and increasing to 1537.4 cm^{-1} at PBE and PBE0, respectively (Table 3).

In total, the discrepancies of the intermediate chain lengths (n = 3−5) are illustrative of their complex electronic structure, which, due to the aforementioned delocalization error and single-determinant representations,[82] DFT and the functionals employed struggle to adequately describe. This mirrors the results observed for the gas phase linked-SEPs where intermediate chains lengths n = 2−4 posed a challenge for the description by the DFT due the significant multi-reference character (to nearly the exact same chain length for *LiAmCn*).

Where the long-chains were characterized as clearly spin-polarized and the intermediate-chains a mixture of competing spin-polarized and spin-unpolarized states, the shortest chains (n = 1−2) suggest a total transition to the spin-unpolarized. For both FHI-aims/PBE and QE/PBE, only the unpolarized state was observed. The band structure of the two closely agree in morphology and predict a metallic character (see Figure 9). For *LiAmC1*, FHI-aims/PBE and QE/PBE disagree only in the Fermi energy; QE shifts the maximum of the conduction band by ∼0.2 eV relative to FHI-aims.

Figure 10 depicts the band structure for *LiAmC4* with a wider energy range accompanied by atomic-projected density of states plots for α and β spins. It is shown that N, C, and H contribute to the bands below the 4 eV, which clearly correspond to the C−H, N−H, and C−N bonds. Li can be fairly represented as Li^+ as its contribution is minimal across the whole energy range. The valence and conduction bands near the Fermi level are dominated by H contributions, as expected since the diffuse electrons are in the periphery of the H centers. In the gas-phase calculations this contribution is provided by the aug-series of basis sets in contrast with the PWs in the periodic DFT calculations. Identical conclusions are made from the atomic-projected density of states for *LiAmC6* and *LiAmC1* which are given in Figures S10 and S11.

A final note remains pertaining to the discussion of magnetic coupling in *LiAmCn*. Supercells (2 × 2 × 2) were constructed for n = 5−7 by repeating the optimized primitive cell twice in the x, y, and z direction to give a supercell containing 16 total SEP centers. FHI-aims/PBE was used for the following results. These were preformed using the tight/tier2 basis set with a uniform 2 × 2 × 2 k-point mesh. Shown in Figure 11 are spin density plots of the three spin states—an antiferromagnetic, a ferromagnetic, and one corresponding to a ferromagnetic state in which the spin of one SEP center has flipped. Comparison of the ferromagnetic and antiferromagnetic states provides a measurement of the J-coupling between the SEP centers. J-coupling was calculated according to refs 83 and 84. For *LiAmC6*, this value is 0.17 K and the energy to spin-flip one center is 0.67 K (see Table S3 of Supporting Information). The ability to computationally isolate specific spin states within bulk *LiAmCn* is an exciting find which offers future avenues of exploration for potential applications of *LiAmCn* in quantum computing and digital storage.

4. SUMMARY AND CONCLUSIONS

In this work, we introduce a new kind of material in which positively charged metal centers linked by diamines are surrounded by diffuse electrons. We specifically employed the Li^+ centers and diamines with hydrocarbon chains of one through ten carbon atoms. We initially considered dimers where two Li^+ centers connected with a single diamine molecule and coordinated to three ammonia molecules each. Then, we expanded our work to a three-dimensional, diamond-like, crystalline structure composed of Li^+ linked with diamines. Our goal was to investigate in detail the electronic structure of the molecular systems and examine the transferability of the findings to the crystalline form.

To aid in description, we introduce a notation referring to the molecular linked-SEPs as *LiAm-LSEP(n)* and the

https://doi.org/10.1021/acs.jpcc.3c00675
J. Phys. Chem. C 2023, 127, 9295−9308

crystalline material composed of linked-SEPs as *LiAmCn*. Here, *Li* refers to the metal identity, *Am* is the type of linkage (amines), and *n* is the length of the aliphatic chain which connects each lithium−amine moiety.

Our work on the molecular dimeric species demonstrated that single determinant methods, specifically DFT, sufficiently describes the species with short and long hydrocarbon chains, but present methodological issues for intermediate lengths. Referring to *LiAm-LSEP(n)*, at CASPT2 the one-carbon chain stabilizes the closed-shell singlets as it favors the coupling of the two electrons in the same orbital. For long chains ($n > 4$), the diradical singlets and triplet states dominate and are nearly degenerate. For chains with two to four carbon atoms, the singlet state reveals strong multi-reference character mixing the closed-shell and diradical electronic configurations. However, DFT does not allow this mixing, as a result, the singlet state changes abruptly from the closed shell to diradical character at the two-carbon chain length and a smaller energy splitting is observed for DFT. At long chain length, for which diradical configurations dominate, DFT better describes the system. For all species, the singlet state is always lower in energy with the splitting decreasing smoothly as the hydrocarbon chain becomes longer. These results on gas-phase molecular linked-SEPs are used as entry point to understand the electronic structure of condensed-phase *LiAmCn*.

To validate the accuracy of DFT calculations of the crystalline linked-SEPs, *LiAmCn*, methodological effects are examined through the comparison of results from two different quantum chemical packages, QE and FHI-aims, and results from different functionals, PBE, PBE0, and B3LYP. Findings therein follow that of *LiAm-LSEP(n)*, demonstrating that gas phase calculations on the *LiAm-LSEP(n)* species provide useful qualitative insights for the *LiAmCn* crystal. Results show that short chains ($n = 1-2$) stabilize the unpolarized solution while the antiferromagnetic is favored for $n > 2$. For short chains, electrons of nearby SEP centers are highly correlated. At long chain lengths, antiferromagnetic and ferromagnetic (singlet and triplet) states become nearly degenerate and electronic bands flatten, indicating minimal electron correlation between nearby SEP centers. Intermediate chain length ($n = 3-5$) represents a transition between unpolarized and spin-polarized descriptions, which poses a significant challenge to descriptions by the DFT.

Comparing methodology, the overall trend of increasing interaction strength between SEP centers with decreasing chain length is agreed by all methods tested though this effect is stronger for QE than FHI-aims. Similarly, the trend of approaching degeneracy of ferromagnetic and antiferromagnetic states with increasing chain length is observed. An agreement is the strongest for the long chains ($n > 5$) and the short chains ($n < 3$). These observations agree with predictions made based on gas phase-linked-SEPs and indicates that gas phase calculations may be used to inform future designs and predictions for SEP-based materials. This offers a benefit in that gas phase calculations may be cheaper computationally and permit use of more accurate quantum chemical methods.

Much work remains to be done in the investigation of *LiAmCn* and SEP-based materials. The present article is intended to provide the first insight into the electronic structure of this material with the aim to spark interest and identify future avenues for the development of quantum technologies and redox catalysts.

■ ASSOCIATED CONTENT

Supporting Information

The Supporting Information is available free of charge at https://pubs.acs.org/doi/10.1021/acs.jpcc.3c00675.

Magnetic moments, energies, electronic band structure, and density of states for the molecular and crystalline species and crystalline cell structure and k-paths used for band structure calculations: https://github.com/JacksonChem/LiAmCn-Files-2023 (PDF)

■ AUTHOR INFORMATION

Corresponding Authors

Stephen G. Dale − *Queensland Micro- and Nanotechnology Centre, Griffith University, Nathan, Queensland 4111, Australia;* orcid.org/0000-0002-6867-711X; Email: stephen.dale@griffith.edu.au

Evangelos Miliordos − *Department of Chemistry and Biochemistry, Auburn University, Auburn, Alabama 36849-5312, United States;* orcid.org/0000-0003-3471-7133; Email: emiliord@auburn.edu

Authors

Benjamin A. Jackson − *Department of Chemistry and Biochemistry, Auburn University, Auburn, Alabama 36849-5312, United States;* orcid.org/0000-0001-6205-8951

María Camarasa-Gómez − *Department of Molecular Chemistry and Materials Science, Weizmann Institute of Science, Rehovoth 7610001, Israel;* orcid.org/0000-0001-9310-8448

Complete contact information is available at: https://pubs.acs.org/10.1021/acs.jpcc.3c00675

Funding

This material is based upon work supported by the National Science Foundation under grant no. CHE-1940456. S.G.D. would like to acknowledge the support of the Australian Government through the Australian Research Council (project number DP200100033). M.C.-G. is grateful to the Azrieli Foundation for the award of an Azrieli International Postdoctoral Fellowship.

Notes

The authors declare no competing financial interest.

■ ACKNOWLEDGMENTS

The authors are indebted to Auburn University (AU) for financial support. E.M. is especially grateful to the donors of the James E. Land endowment. This work was completed with resources provided by the Auburn University Hopper and Easley Clusters. B.A.J. would like to acknowledge the support of the U.S. Department of Energy through the Office of Science Graduate Student Research Program. We are finally grateful to Dr. Isuru Ariyarathna for the valuable and insightful discussions.

■ REFERENCES

(1) Ibberson, R. M.; Fowkes, A. J.; Rosseinsky, M. J.; David, W. I. F.; Edwards, P. P. Structure and Phase Behavior of the Expanded-Metal Compound $^{7}Li(ND_3)_4$. *Angew. Chem., Int. Ed.* **2009**, *48*, 1435−1438.

(2) Seel, A. G.; Zurek, E.; Ramirez-Cuesta, A. J.; Ryan, K. R.; Lodge, M. T. J.; Edwards, P. P. Low Energy Structural Dynamics and Constrained Libration of $Li(NH_3)_4$, the Lowest Melting Point Metal. *Chem. Commun.* **2014**, *50*, 10778−10781.

(3) Stacy, A. M.; Sienko, M. J. Reevaluation of the Crystal Structure Data on the Expanded-Metal Compounds $Li(NH_3)_4$ and $Li(ND_3)_4$. *Inorg. Chem.* **1982**, *21*, 2294−2297.
(4) Dye, J. L. Electrons as Anions. *Science* **2003**, *301*, 607−608.
(5) Liu, C.; Nikolaev, S. A.; Ren, W.; Burton, L. A. Electrides: A Review. *J. Mater. Chem. C* **2020**, *8*, 10551−10567.
(6) Almeida, N. M. S.; Pawłowski, F.; Ortiz, J. V.; Miliordos, E. Transition-metal Solvated-electron Precursors: Diffuse and 3d Electrons in $V(NH_3)_6^{0,\pm}$. *Phys. Chem. Chem. Phys.* **2019**, *21*, 7090−7097.
(7) Ariyarathna, I. R.; Almeida, N. M. S.; Miliordos, E. Stability and Electronic Features of Calcium Hexa-Hepta-and Octa-Coordinated Ammonia Complexes: A First-Principles Study. *J. Phys. Chem. A* **2019**, *123*, 6744−6750.
(8) Sommerfeld, T.; Dreux, K. M. Characterizing the Excess Electron of $Li(NH_3)_4$. *J. Chem. Phys.* **2012**, *137*, 244302.
(9) Dawes, S. B.; Eglin, J. L.; Moeggenborg, K. J.; Kim, J.; Dye, J. L. Cs^+(15-crown-5)2.e^-. A Crystalline Antiferromagnetic Electride. *J. Am. Chem. Soc.* **1991**, *113*, 1605−1609.
(10) Almeida, N. M. S.; Miliordos, E. Electronic and Structural Features of Octa-coordinated Yttrium−ammonia Complexes: The First Neutral Solvated Electron Precursor With Eight Ligands and Three Outer Electrons. *Phys. Chem. Chem. Phys.* **2019**, *21*, 7098−7104.
(11) Ariyarathna, I. R.; Khan, S. N.; Pawłowski, F.; Ortiz, J. V.; Miliordos, E. Aufbau Rules for Solvated Electron Precursors: $Be(NH_3)_4^{0,\pm}$ Complexes and Beyond. *J. Phys. Chem. Lett.* **2018**, *9*, 84−88.
(12) Jackson, B. A.; Miliordos, E. Electronic and Geometric Structure of Cationic and Neutral Chromium and Molybdenum Ammonia Complexes. *J. Chem. Phys.* **2021**, *155*, 014303.
(13) Khan, S. N.; Miliordos, E. Scandium in Neutral and Positively Charged Ammonia Complexes: Balancing between Sc2+ and Sc3+. *J. Phys. Chem. A* **2020**, *124*, 4400−4412.
(14) Jordan, Z.; Khan, S. N.; Jackson, B. A.; Miliordos, E. Can Boron Form Coordination Complexes with Diffuse Electrons? Evidence for Linked Solvated Electron Precursors. *Electron. Struct.* **2022**, *4*, 015001.
(15) Zurek, E.; Edwards, P. P.; Hoffmann, R. A Molecular Perspective on Lithium−Ammonia Solutions. *Angew. Chem., Int. Ed.* **2009**, *48*, 8198−8232.
(16) Albaqami, M. D.; Ellis, A. M. Infrared Spectroscopy of $Ca(NH_3)_n$ Complexes. *Chem. Phys. Lett.* **2018**, *706*, 736−740.
(17) Takasu, R.; Misaizu, F.; Hashimoto, K.; Fuke, K. Microscopic Solvation Process of Alkali Atoms in Finite Clusters: Photoelectron and Photoionization Studies of M(NH3)n and $M(H_2O)_n$ (M = Li, Li^-, Na^-). *J. Phys. Chem. A* **1997**, *101*, 3078−3087.
(18) Berg, C.; Achatz, U.; Beyer, M.; Joos, S.; Albert, G.; Schindler, T.; Niedner-Schatteburg, G.; Bondybey, V. E. Chemistry and Charge Transfer Phenomena in Water Cluster Cations. *Int. J. Mass Spectrom. Ion Processes* **1997**, *167−168*, 723−734.
(19) Harms, A. C.; Khanna, S. N.; Chen, B.; Castleman, A. W. Dehydrogenation Reactions in $Mg^+(H_2O)_n$ Clusters. *J. Chem. Phys.* **1994**, *100*, 3540−3544.
(20) Reinhard, B. M.; Niedner-Schatteburg, G. Co-Existence of Hydrated Electron and Metal di-Cation in $[Mg(H_2O)_n]^+$. *Phys. Chem. Chem. Phys.* **2002**, *4*, 1471−1477.
(21) Mason, P. E.; Schewe, H. C.; Buttersack, T.; Kostal, V.; Vitek, M.; McMullen, R. S.; Ali, H.; Trinter, F.; Lee, C.; Neumark, D. M.; et al. Spectroscopic Evidence for a Gold-Coloured Metallic Water Solution. *Nature* **2021**, *595*, 673−676.
(22) Barnes, J. V.; Yoder, B. L.; Signorell, R. Magic Numbers for the Photoelectron Anisotropy in Li-Doped Dimethyl Ether Clusters. *J. Phys. Chem. A* **2019**, *123*, 2379−2386.
(23) West, A. H. C.; Yoder, B. L.; Luckhaus, D.; Saak, C.-M.; Doppelbauer, M.; Signorell, R. Angle-Resolved Photoemission of Solvated Electrons in Sodium-Doped Clusters. *J. Phys. Chem. Lett.* **2015**, *6*, 1487−1492.
(24) Ariyarathna, I. R.; Miliordos, E. Ground and Excited States Analysis of Alkali Metal Ethylenediamine and Crown Ether Complexes. *Phys. Chem. Chem. Phys.* **2021**, *23*, 20298−20306.
(25) Dawes, S. B.; Ward, D. L.; Huang, R. H.; Dye, J. L. First Electride Crystal Structure. *J. Am. Chem. Soc.* **1986**, *108*, 3534−3535.
(26) Ellaboudy, A.; Dye, J. L.; Smith, P. B. Cesium 18-crown-6 Compounds. A Crystalline Ceside and a Crystalline Electride. *J. Am. Chem. Soc.* **1983**, *105*, 6490−6491.
(27) Mones, L.; Pohl, G.; Turi, L. Ab Initio Molecular Dynamics Study of Solvated Electrons in Methanol Clusters. *Phys. Chem. Chem. Phys.* **2018**, *20*, 28741−28750.
(28) Walker, J. A.; Bartels, D. M. A Simple ab Initio Model for the Solvated Electron in Methanol. *J. Phys. Chem. A* **2016**, *120*, 7240−7247.
(29) Ariyarathna, I. R. Superatomic Chelates: The Cases of Metal Aza-Crown Ethers and Cryptands. *Inorg. Chem.* **2022**, *61*, 579−585.
(30) Edwards, P. P.; Lusis, A. R.; Sienko, M. J. Conduction- and Localized Electron Spin Resonance in the Lithium−methylamine System: Inferences for the Existence of the Metallic Compound Tetramethylaminelithium(zero), $Li(CH_3NH_2)_4$. *J. Chem. Phys.* **1980**, *72*, 3103−3112.
(31) Hagedorn, R.; Sienko, M. J. Conductivity Studies in Search of Liquid-liquid Phase Separation by Solutions of Lithium in Methylamine. *J. Phys. Chem.* **1982**, *86*, 2094−2097.
(32) Hayama, S.; Wasse, J. C.; Skipper, N. T.; Soper, A. K. Structure of Solutions of Lithium in Methylamine across the Metal−Nonmetal Transition. *J. Phys. Chem. B* **2002**, *106*, 11−14.
(33) Maeda, K.; Lodge, M. T. J.; Harmer, J.; Freed, J. H.; Edwards, P. P. Electron Tunneling in Lithium−Ammonia Solutions Probed by Frequency-Dependent Electron Spin Relaxation Studies. *J. Am. Chem. Soc.* **2012**, *134*, 9209−9218.
(34) Nakamura, Y.; Niibe, M.; Shimoji, M. NMR Study of Lithium in Liquid Ammonia and Methylamine. *J. Phys. Chem.* **1984**, *88*, 3755−3760.
(35) Seel, A. G.; Swan, H.; Bowron, D. T.; Wasse, J. C.; Weller, T.; Edwards, P. P.; Howard, C. A.; Skipper, N. T. Electron Solvation and the Unique Liquid Structure of a Mixed-Amine Expanded Metal: The Saturated Li−NH3−MeNH2 System. *Angew. Chem., Int. Ed.* **2017**, *56*, 1561−1565.
(36) Stacy, A. M.; Johnson, D. C.; Sienko, M. J. Low Temperature Magnetic Susceptibility of the Expanded Metal Compounds $Li(NH_3)_4$, $Li(ND_3)_4$, and $Li(CH_3NH_2)_4$. *J. Chem. Phys.* **1982**, *76*, 4248−4254.
(37) Thompson, H.; Wasse, J. C.; Skipper, N. T.; Hayama, S.; Bowron, D. T.; Soper, A. K. Structural Studies of Ammonia and Metallic Lithium−Ammonia Solutions. *J. Am. Chem. Soc.* **2003**, *125*, 2572−2581.
(38) Jackson, B. A.; Miliordos, E. The Nature of Supermolecular Bonds: Investigating Hydrocarbon Linked Beryllium Solvated Electron Precursors. *J. Chem. Phys.* **2022**, *156*, 194302.
(39) Zurek, E.; Wen, X.-D.; Hoffmann, R. (Barely) Solid Li(NH3)4: The Electronics of an Expanded Metal. *J. Am. Chem. Soc.* **2011**, *133*, 3535−3547.
(40) Birch, A. J. 117. Reduction by dissolving metals. Part I. *J. Chem. Soc.* **1944**, 430−436.
(41) Hwu, J. R.; Wein, Y. S.; Leu, Y.-J. Calcium Metal in Liquid Ammonia for Selective Reduction of Organic Compounds. *J. Org. Chem.* **1996**, *61*, 1493−1499.
(42) Jackson, B. A.; Miliordos, E. Simultaneous CO_2 Capture and Functionalization: Solvated Electron Precursors as Novel Catalysts. *Chem. Commun.* **2022**, *58*, 1310−1313.
(43) Adams, C. S.; Pritchard, J. D.; Shaffer, J. P. Rydberg Atom Quantum Technologies. *J. Phys. B: At., Mol. Opt. Phys.* **2020**, *53*, 012002.
(44) Spong, N. L. R.; Jiao, Y.; Hughes, O. D. W.; Weatherill, K. J.; Lesanovsky, I.; Adams, C. S. Collectively Encoded Rydberg Qubit. *Phys. Rev. Lett.* **2021**, *127*, 063604.
(45) Wu, X.; Liang, X.; Tian, Y.; Yang, F.; Chen, C.; Liu, Y.-C.; Tey, M. K.; You, L. A Concise Review of Rydberg Atom Based Quantum

Computation and Quantum Simulation. *Chin. Phys. B* **2021**, *30*, 020305.
(46) Gaita-Ariño, A.; Luis, F.; Hill, S.; Coronado, E. Molecular Spins for Quantum Computation. *Nat. Chem.* **2019**, *11*, 301−309.
(47) Lehmann, J.; Gaita-Ariño, A.; Coronado, E.; Loss, D. Quantum Computing with Molecular Spin Systems. *J. Mater. Chem.* **2009**, *19*, 1672−1677.
(48) Bayliss, S. L.; Laorenza, D. W.; Mintun, P. J.; Kovos, B. D.; Freedman, D. E.; Awschalom, D. D. Optically Addressable Molecular Spins for Quantum Information Processing. *Science* **2020**, *370*, 1309−1312.
(49) Hernangómez-Pérez, D.; Gunasekaran, S.; Venkataraman, L.; Evers, F. Solitonics with Polyacetylenes. *Nano Lett.* **2020**, *20*, 2615−2619.
(50) Park, J. W.; Do, E.; Shin, J. S.; Song, S. K.; Stetsovych, O.; Jelinek, P.; Yeom, H. W. Creation and Annihilation of Mobile Fractional Solitons in Atomic Chains. *Nat. Nanotechnol.* **2022**, *17*, 244−249.
(51) Hötger, A.; Amit, T.; Klein, J.; Barthelmi, K.; Pelini, T.; Delhomme, A.; Rey, S.; Potemski, M.; Faugeras, C.; Cohen, G., et al. Spin-defect Characteristics of Single Sulfur Vacancies in Monolayer MoS_2. **2022**, arXiv:2205.10286.
(52) Yanai, T.; Tew, D. P.; Handy, N. C. A New Hybrid Exchange−Correlation Functional Using the Coulomb-Attenuating Method (CAM-B3LYP). *Chem. Phys. Lett.* **2004**, *393*, 51−57.
(53) Dunning, T. H. Gaussian Basis Sets for Use in Correlated Molecular Calculations. I. The Atoms Boron Through Neon and Hydrogen. *J. Chem. Phys.* **1989**, *90*, 1007−1023.
(54) Kendall, R. A.; Dunning, T. H.; Harrison, R. J. Electron Affinities of the First-row Atoms Revisited. Systematic Basis Sets and Wave Functions. *J. Chem. Phys.* **1992**, *96*, 6796−6806.
(55) Woon, D. E.; Dunning, T. H. Gaussian Basis Sets for Use in Correlated Molecular Calculations. IV. Calculation of Static Electrical Response Properties. *J. Chem. Phys.* **1994**, *100*, 2975−2988.
(56) Ariyarathna, I. R.; Pawłowski, F.; Ortiz, J. V.; Miliordos, E. Aufbau Principle for Diffuse Electrons of Double-Shell Metal Ammonia Complexes: The Case of $M(NH_3)_4@12NH_3$, M = Li, Be^+, B^{2+}. *J. Phys. Chem. A* **2020**, *124*, 505−512.
(57) Werner, H.-J.; Knowles, P. J.; Knizia, G.; Manby, F. R.; Schütz, M.; Celani, P.; Györffy, W.; Kats, D.; Korona, T.; Lindh, R., et al. *MOLPRO*, version 2015.1, a package of ab initio programs, 2015.
(58) Ghigo, G.; Roos, B. O.; Malmqvist, P.-A. A Modified Definition of the Zeroth-order Hamiltonian in Multiconfigurational Perturbation Theory (CASPT2). *Chem. Phys. Lett.* **2004**, *396*, 142−149.
(59) Roos, B. O.; Andersson, K. Multiconfigurational Perturbation Theory with Level Shift — The Cr_2 Potential Revisited. *Chem. Phys. Lett.* **1995**, *245*, 215−223.
(60) Becke, A. D. Density-functional Thermochemistry III: The Role of Exact Exchange. *J. Chem. Phys.* **1993**, *98*, 5648−5652.
(61) Stephens, P. J.; Devlin, F. J.; Chabalowski, C. F.; Frisch, M. J. Ab Initio Calculation of Vibrational Absorption and Circular Dichroism Spectra Using Density Functional Force Fields. *J. Phys. Chem.* **1994**, *98*, 11623−11627.
(62) Perdew, J. P.; Burke, K.; Ernzerhof, M. Generalized Gradient Approximation Made Simple. *Phys. Rev. Lett.* **1996**, *77*, 3865−3868.
(63) Frisch, M. J.; Trucks, G. W.; Schlegel, H. B.; Scuseria, G. E.; Robb, M. A.; Cheeseman, J. R.; Scalmani, G.; Barone, V.; Petersson, G. A.; Nakatsuji, H., et al. *Gaussian 16*, Revision A.03, 2016.
(64) Giannozzi, P.; Baroni, S.; Bonini, N.; Calandra, M.; Car, R.; Cavazzoni, C.; Ceresoli, D.; Chiarotti, G. L.; Cococcioni, M.; Dabo, I.; et al. QUANTUM ESPRESSO: a Modular and Open-source Software Project for Quantum Simulations of Materials. *J. Phys.: Condens. Matter* **2009**, *21*, 395502.
(65) Blum, V.; Gehrke, R.; Hanke, F.; Havu, P.; Havu, V.; Ren, X.; Reuter, K.; Scheffler, M. Ab Initio Molecular Simulations With Numeric Atom-centered Orbitals. *Comput. Phys. Commun.* **2009**, *180*, 2175−2196.
(66) Blöchl, P. E. Projector Augmented-wave Method. *Phys. Rev. B: Condens. Matter Mater. Phys.* **1994**, *50*, 17953−17979.
(67) Johnson, E. R.; Otero-de-la-Roza, A.; Dale, S. G. Extreme Density-driven Delocalization Error for a Model Solvated-electron System. *J. Chem. Phys.* **2013**, *139*, 184116.
(68) Lejaeghere, K.; Bihlmayer, G.; Björkman, T.; Blaha, P.; Blügel, S.; Blum, V.; Caliste, D.; Castelli, I. E.; Clark, S. J.; Dal Corso, A.; et al. Reproducibility in Density Functional Theory Calculations of Solids. *Science* **2016**, *351*, aad3000.
(69) Zhao, Q.; Kulik, H. J. Where Does the Density Localize in the Solid State? Divergent Behavior for Hybrids and DFT+U. *J. Comput. Theor. Chem.* **2018**, *14*, 670−683.
(70) Pulay, P. Convergence Acceleration of Iterative Sequences. the Case of SCF Iteration. *Chem. Phys. Lett.* **1980**, *73*, 393−398.
(71) de Gelder, R.; Wehrens, R.; Hageman, J. A. A Generalized Expression for the Similarity of Spectra: Application to Powder Diffraction Pattern Classification. *J. Comput. Chem.* **2001**, *22*, 273−289.
(72) Otero-de-la-Roza, A.; Johnson, E. R.; Luaña, V. Critic2: A Program for Real-Space Analysis of Quantum Chemical Interactions in Solids. *Comput. Phys. Commun.* **2014**, *185*, 1007−1018.
(73) Kokalj, A. XCrySDen—a New Program for Displaying Crystalline Structures and Electron Densities. *J. Mol. Graphics Modell.* **1999**, *17*, 176−179.
(74) Humphrey, W.; Dalke, A.; Schulten, K. VMD: Visual Molecular Dynamics. *J. Mol. Graphics* **1996**, *14*, 33−38.
(75) Knizia, G. Intrinsic Atomic Orbitals: An Unbiased Bridge between Quantum Theory and Chemical Concepts. *J. Comput. Theor. Chem.* **2013**, *9*, 4834−4843.
(76) Miliordos, E.; Ruedenberg, K.; Xantheas, S. S. Unusual Inorganic Biradicals: A Theoretical Analysis. *Angew. Chem., Int. Ed.* **2013**, *52*, 5736−5739.
(77) Olivares-Pilón, H.; Turbiner, A. V. H_2^+, HeH and H_2: Approximating Potential Curves, Calculating Rovibrational States. *Ann. Phys.* **2018**, *393*, 335−357.
(78) Sharp, T. E. Potential-Energy Curves for Molecular Hydrogen and its Ions. *At. Data Nucl. Data Tables* **1970**, *2*, 119−169.
(79) Hayes, E. F.; Siu, A. K. Q. Electronic Structure of the Open Forms of Three-membered Rings. *J. Am. Chem. Soc.* **1971**, *93*, 2090−2091.
(80) Laidig, W. D.; Schaefer, H. F. Large Multiconfiguration Self-Consistent-Field Wave Functions for the Ozone Molecule. *J. Chem. Phys.* **1981**, *74*, 3411−3414.
(81) Gräfenstein, J.; Kraka, E.; Cremer, D. Effect of the Self-interaction Error for Three-electron bonds: On the Development of New exchange-correlation Functionals. *Phys. Chem. Chem. Phys.* **2004**, *6*, 1096−1112.
(82) Bryenton, K. R.; Adeleke, A. A.; Dale, S. G.; Johnson, E. R. Delocalization Error: The Greatest Outstanding Challenge in Density-Functional Theory. *Wiley Interdiscip. Rev. Comput. Mol. Sci.* **2022**, *13*, No. e1631.
(83) Ryabinkin, I. G.; Staroverov, V. N. Interelectron Magnetic Coupling in Electrides with One-Dimensional Cavity-Channel Geometry. *Phys. Chem. Chem. Phys.* **2011**, *13*, 21615−21620.
(84) Soda, T.; Kitagawa, Y.; Onishi, T.; Takano, Y.; Shigeta, Y.; Nagao, H.; Yoshioka, Y.; Yamaguchi, K. Ab Initio Computations of Effective Exchange Integrals for H−H, H−He−H and Mn_2O_2 Complex: Comparison of Broken-Symmetry Approaches. *Chem. Phys. Lett.* **2000**, *319*, 223−230.

https://doi.org/10.1021/acs.jpcc.3c00675
J. Phys. Chem. C 2023, 127, 9295−9308